LS-OPT® Status Update

Nielen Stander[1], Anirban Basudhar[1], Imtiaz Gandikota[1],

Katharina Liebold[2], Åke Svedin[2], Charlotte Keisser[2]

[1]LST LLC, Ansys, Livermore, CA

[2]DYNAmore GmbH, Stuttgart-Vaihingen, BRD

1 Introduction

LS-OPT Version 7.0 was released in November 2020 with several new features which are briefly summarized here:

- *Job scheduler.* The job scheduler for distributing simulation and other runs is a complete redesign. It includes SSH Proxy, new Blackbox features and new GUI dialogs. It also supports user options for normal, error and abnormal termination when employing user-defined solvers.
- *Principal Component Analysis.* This new methodology can be applied to histories and response fields for the purpose of sensitivity analysis. Graphical post-processing features are available.
- *Process management* often involves disabling and enabling stages so that cases or stages can be run independently, e.g., for debugging the setup, for testing load cases independently or in a scenario where individual designers are responsible for specific stages. A new GUI feature, which grays out disabled stages or cases, accompanies this new utility.
- *Classifier-based sampling constraints* for adaptive sampling. This can be used to define adaptively refined sampling domains for probabilistic analysis or optimization. Thus, sampling of irrelevant design space regions is avoided to reduce the number of function evaluations and more samples are added to important regions to improve accuracy. For instance, samples can be added in the vicinity of the constraint boundary for reliability analysis to obtain higher accuracy of the constraint approximation.
- *Sequential* metamodel-based probabilistic analysis. In previous LS-OPT versions, probabilistic analysis (Monte Carlo task) was limited to a single iteration. In version 7.0, probabilistic analysis (Metamodel-based Monte Carlo) can be performed iteratively to obtain convergence statistics and termination criteria can be defined based on failure probability value and/or response accuracy. The iterative analysis can be done in conjunction with classifier-based adaptive sampling constraints, also added in the same version.
- Material parameter identification typically involves comparing noisy, and occasionally hysteretic, curves of different lengths. E.g., the test curve only spans part of the computed curve produced by the solver. In an earlier version, the Dynamic Time Warping method [1,2,3,4] was introduced to address noise and hysteresis. Version 7 features a modified DTW method, *DTW-p,* for improving material identification accuracy for partial curve matching [5].
- *Distribution fitting* (Normal and Weibull) using user-defined observation data.
- An interface to *Oasys PRIMER.*

These features represent the last update of the original ‘free‘ version of LS-OPT developed since 1998. The development over the last year has emphasized integration with Ansys products. Among other developments, this involves the transfer of features to and from the optimization code optiSLang. Part of this integration involves the introduction of the Metamodel of Optimal Prognosis [6], an automated metamodel selection method introduced in optiSLang, into LS-OPT Pro. A vehicle crash example is presented here to demonstrate some of the capabilities in comparison with LS-OPT metamodels. As part of the integration process, several LS-OPT features are also being transferred to optiSLang.

The enhanced product, *LS-OPT Pro,* will be licensed as an *Ansys-LST* product.

2 *LS-OPT Pro* Release 2022 R1

A new version of LS-OPT will be released early 2022 as a licensed *LS-OPT Pro 2022-R1*. This means that LS-OPT becomes part of a 3-tier series of optimization programs featuring LS-OPT Pro – optiSLang Premium – optiSLang Enterprise. LS-OPT Pro has the following main new features:

- ***Point Mapping**:* In addition to quadrilateral shells, point-based mapping has been extended to triangular shell elements) as well as most solid elements supported by LS-DYNA (hexahedron, pentahedron, tetrahedron. This is a useful feature since most meshes are not uniform and automatic meshers often use tetrahedra (for solids) or triangles (for shells). This feature allows extraction of results at arbitrary spatial locations that need not coincide with nodal points. The mapping applies to responses, histories, multi-point histories and multi-point responses (fields). The applications are in Digital Image Correlation (DIC) and Magnetic Resonance Imaging (MRI).
- ***LS-OPT Extractor**:* The Extractor has always been a standalone executable. This has allowed for easy integration of LS-DYNA into other Ansys products. In addition to direct extraction, crash criteria, mathematical expressions and other special functions such as similarity measures are made available. The Extractor is now supported with a GUI to define the extraction commands.
- ***LS-Reader*** integration: LS-Reader is a comprehensive LS-DYNA interface developed by the LS-PrePost group. This interface has now replaced the native LS-OPT/LS-DYNA interface for reasons of robustness and being comprehensive and up-to-date. The previous versions of LS-OPT haven't always kept up with new developments resulting in occasional extraction failures. This issue is now resolved in the new interface. Currently only the *d3plot* interface has been replaced, this being the major part of LS-Reader. LS-Reader is integrated with the aforementioned standalone Extractor, as well as *LS-TaSC*. The plan is to expand the current LS-DYNA interface in LS-OPT to support all the result types available in LS-Reader such as Acoustics, SPH, CFD, etc.
- ***A CORA interface*** has been added for seamless integration of ISO 18571 standard rating for dummies and barriers [7] into an LS-OPT process flow. The response interface allows the extraction of similarity measures for individual load cases, signals and injury criteria or for all of them together. The overall rating is a weighted sum of measures from different approaches, such as the corridor method, correlation method etc. The CORA interface is selected as a stage type.
- ***Metamodel of Optimal Prognosis (MOP)***. This is a metamodel-based method, integrated from optiSLang (an Ansys product), which relies on the automatic selection of metamodels [6]. Future versions will integrate all the metamodels currently available in LS-OPT (Polynomials, Feedforward Neural Networks, Radial Basis Function Networks, Support Vector Regression) into an extended MOP feature (referred to as MOP-X). This automates the selection from a wide array of models.

3 Example

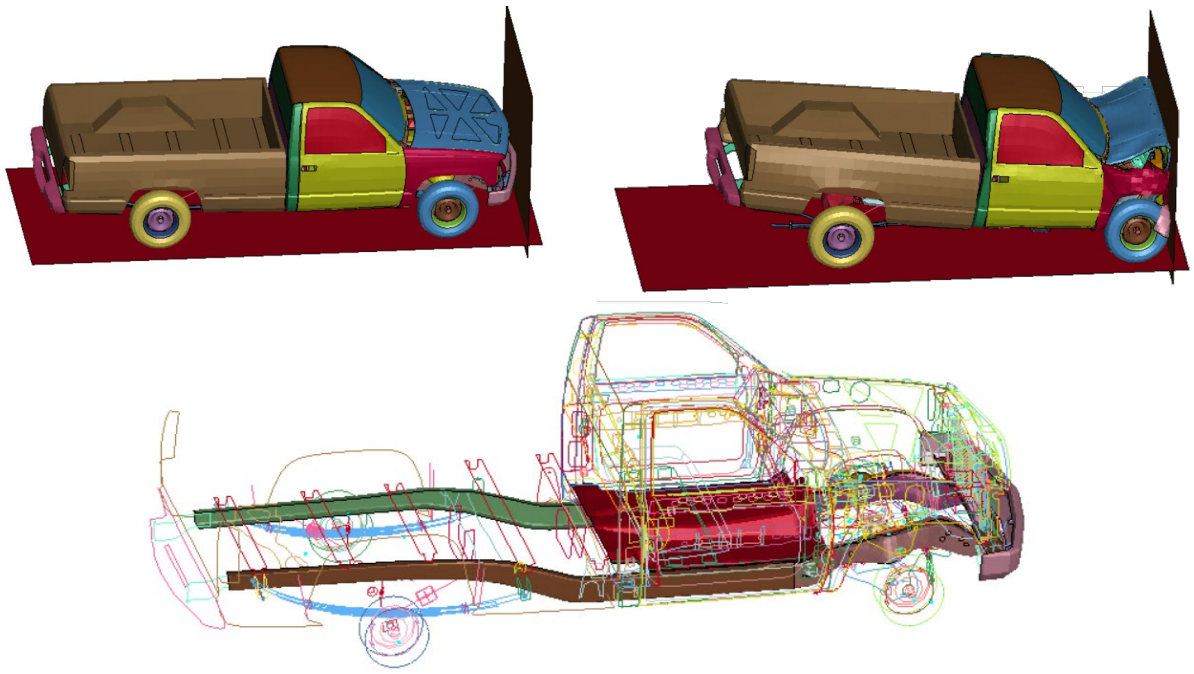

Fig.1: Truck frontal impact showing design components (NHTSA)

3.1 Truck, frontal impact with 6 variables

Intrusions and pulses of a truck impact example were used to compare the accuracy of the MOP-selected metamodel with selected LS-OPT metamodels Radial Basis Functions (RBF), Feedforward Neural Networks (FFNN) and Kriging. The pulses are acceleration related quantities computed over two time intervals of the crash event. The design optimization problem is stated as follows:

$$\begin{aligned} \min \quad & Scaled\ Mass \\ s.t. \quad & Scaled\ Displacement \le 1 \\ & Scaled\ Stage1\ Pulse \le 1 \\ & Scaled\ Stage2\ Pulse \le 1 \end{aligned}$$

Table 1 represents the results of a 6-variable problem including 6 thickness variables of grouped part thicknesses. Table 2 represents a 22-variable problem which uses 11 part thickness variables and 11 material properties of the corresponding parts. In each case a number of test points larger than the number of construction points was used to quantify the metamodel prediction accuracy. The root mean square errors at the independent test points have been highlighted with the lowest value italicized and boldfaced. As a control, a direct optimization, using the GA algorithm, was also conducted. 25 Iterations with a population of 30 each were run using the 6-variable problem while 20 iterations with a population of 100 each were executed using the 22-variable problem.

	RBF	***FFNN***	***Kriging***	***MOP***	***MOP***	***GA Direct Optimum***
	Predicted	*Predicted*	*Predicted*	*Predicted*	*Model*	*Computed*
Optimal variable values						
t1, t3	2.876	2.832	2.925	2.84		2.541
t2, t4	2.398	2.407	2.524	2.517		2.982
t5, t6	2.72	2.72	2.72	2.72		2.725
t10	2.16	2.162	2.16	2.16		2.166
t64	1.455	1.396	1.096	1.139		1.045
t73	1.592	1.592	1.592	1.592		1.594
RMS fitting error and Optimal response values						
N1_disp	724.8	722.9	722.8	725	Kriging	723
RMS	6.85	***5.89***	8.66	6.47		
N2_disp	725.3	727.3	727.3	725.2	Kriging	724.9
RMS	6.58	***5.51***	8.53	6		
Stage1_pulse	7.037	7.006	7.027	7.121	Linear	6.99
RMS	***0.0482***	0.0489	0.057	0.109		
Stage2_pulse	19.24	19.01	19.82	19.49	Linear	20.16
RMS	0.27	***0.251***	0.355	0.383		
Objective (mass) and constraint values						
scaled_mass	0.825	0.823	0.827	0.826		0.829
scaled_disp	1	1	1	1		1
scaled_stage1_pulse	0.930	0.928	0.929	0.941		0.924
scaled_stage2_pulse	0.907	0.894	0.936	0.919		0.951

Table 1: The LS-OPT Pro and MOP fitting (highlighted) and optimization results for the truck frontal impact. The optimization problem has 6 thickness sizing variables. The lowest RMS error values are highlighted in italic bold. The metamodel was built using 400 sampling points with the RMS error evaluated at 600 independent test points. The metamodels selected by the MOP system are also shown.

3.2 Truck, frontal impact with 22 variables

	RBF	***FFNN***	***Kriging***	***MOP***	***MOP***	***GA Direct Optimum***
	Predicted	*Predicted*	*Predicted*	*Predicted*	*Model*	*Computed*
Optimal variable values						
t1, m1	2.510, 298.6	2.510, 325.7	2.510, 338.5	2.510, 205.9		2.920, 204.4
t2, m2	2.398, 293.3	2.398, 190.8	2.398, 228.5	2.398, 340.5		2.467, 309.2
t3 , m3	2.510, 245.7	2.510, 288.3	2.510, 310.0	2.510, 321.6		2.623, 266.1
t4, m4	2.399, 259.5	2.399, 280.2	2.399, 256.3	2.399, 290.2		2.588, 184.5
t5, m5	2.721, 194.3	2.721, 310.7	2.721, 183.3	2.721, 278.2		2.784, 191.7
t6, m6	2.721, 265.4	2.721, 180.1	2.721, 181.3	2.721, 319.6		2.725, 183.9
t10, m10	2.162, 254.1	2.162, 180.2	2.162, 329.2	2.162, 309.1		2.210, 194.0
t11, m11	2.440, 320.2	3.600, 312.3	3.379, 337.3	2.784, 217.7		2.566, 194.7
t12, m12	2.652, 286.3	2.752, 349.7	2.484, 234.4	2.883, 348.3		2.761, 181.6
t64, m64	1.010, 180.1	1.010, 180.1	1.010, 247.0	1.229, 340.2		1.047, 187.3
t73, m73	1.593, 318.2	1.593, 345.0	1.593, 321.7	1.593, 333.3		1.614, 319.7
RMS fitting error and Optimal response values						
N1_disp	721.2	724.4	721.9	723.6	Linear	719.06
RMS	7.75	***5.89***	8.03	8.14		
N2_disp	721.6	725.6	720.5	721.6	Linear	718.55
RMS	7.37	***5.69***	7.90	7.8		
Stage1 pulse	6.389	6.256	7.518	7.141	Linear	5.49
RMS	0.0686	***0.0653***	0.129	0.166		
Stage2 pulse	19.940	20.970	19.18	20.19	Linear	19.25
RMS	***0.3450***	0.3570	0.383	0.521		
HIC	-6.88e+04	-4.885e+05	-2.13e+05	1.24e+05	Linear	5.013e+04
RMS	***4.24e+05***	1.04e+06	4.41e+05	4.56e+05		
Objective (mass) and constraint values						
scaled_mass	0.8006	0.8000	0.8006	0.8051		0.8272
scaled_disp	0.9951	1.0000	0.9948	0.9967		0.9914
scaled_stage1 pulse	0.8451	0.8276	0.9945	0.9446		0.7264
scaled_stage2 pulse	0.9407	0.9891	0.9045	0.9522		0.9082

Table 2: LS-OPT Pro and MOP fitting (highlighted) and optimization results for the truck frontal impact. The optimization problem has 11 thickness sizing variables and 11 corresponding part material variables. The lowest RMS error values are highlighted in italic bold. The metamodel was built using 800 sampling points with the RMS error evaluated at 1200 independent test points. The metamodels selected by the MOP system are also shown.

The tables demonstrate the advantage of extending the MOP feature, especially by adding the Feedforward Neural Network metamodel. Note that the *HIC* prediction accuracy remains very poor (RMS error typically larger than the magnitude) presumably due to its highly nonlinear behavior.

Two smaller 2-variable crash examples were also tested, displaying results in which the current MOP feature outperformed the LS-OPT options for some responses. Smaller examples may be less representative of an industrial environment but the results collectively illustrate the potential benefit of automatic selection of the best metamodel for each response as well as extending the MOP strategy (MOP-X) to include the LS-OPT metamodels (see also 4.1 below).

4 LS-OPT Pro Outlook (2022 R2)

Another version of LS-OPT (2022 R2) will be released in the second half of next year. Several new features for this version are currently under development and some are nearing completion. Some of the prominent features are as follows.

4.1 Extended MOP

The MOP feature imported from optiSLang was presented in sections 2 and 3. It has the advantage of not having to manually select the metamodel type, but is limited in the choice of candidate metamodel types. 2022 R2 LS-OPT Pro version will consist of an enhanced MOP with *Feedforward Neural Networks*, *Radial Basis Function Networks*, *Support Vector Regression* and *Support Vector Classification* as additional choices for automatically selecting the best candidate.

4.2 Adaptive Multi-objective Optimization (MOO)

2022 R2 will also include an adaptive sequential MOO method in addition to the current direct NSGA-II and metamodel-based (non-adaptive) sequential method. This will be based on a patented classifier-based method referred to as Adaptive Explicit Multi-objective Optimization (AEMOO) [9]. It has been shown to be a fast and robust approach compared to current methods [10]. A comparative study is provided here for the current state of AEMOO implementation that is still missing some algorithm steps. The final release will contain a more robust and efficient implementation that will include those steps. The example used involves a simplified car model with frontal crash. Mass and intrusion are minimized while applying a constraint on a Head Injury Criterion (HIC) value.

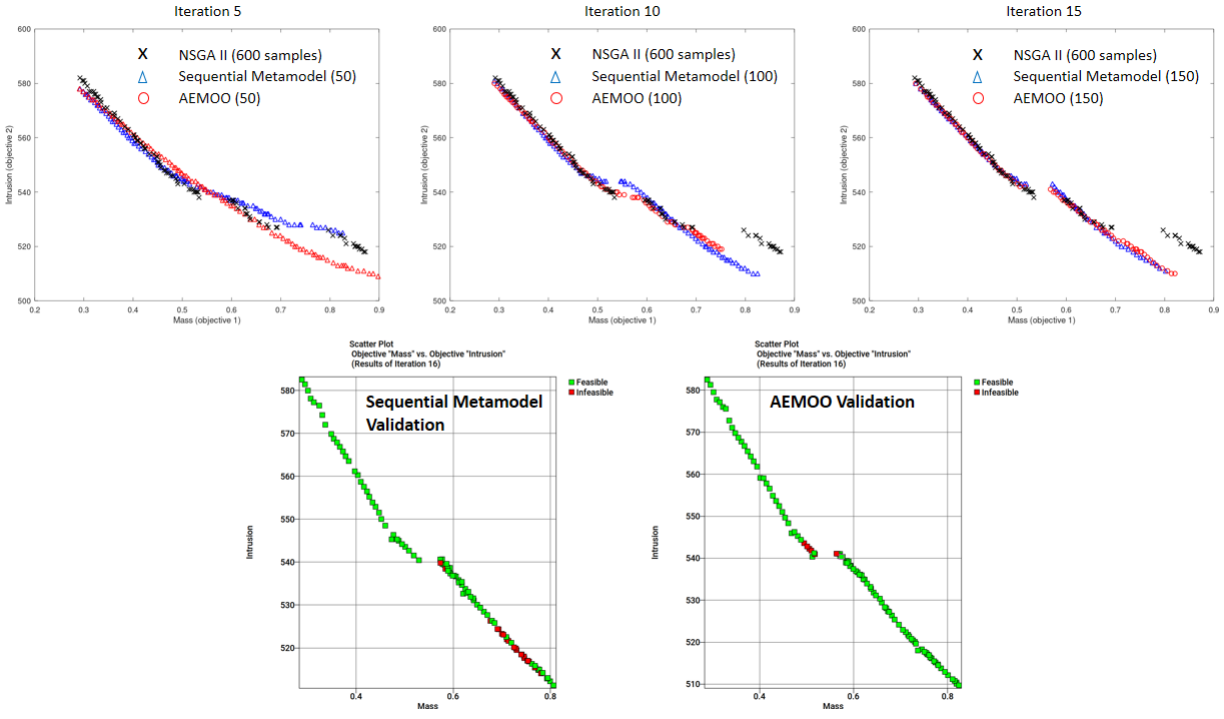

Fig.2: Comparison of predicted Pareto Optimal fronts using sequential metamodel-based optimization (blue triangles) and AEMOO (red circles) to the computed front using 600 point direct NSGA-II-based optimization (top). 10 points per iteration were used for both sequential metamodeling and AEMOO. The bottom figures depict the validation results for the Pareto Optimal fronts obtained using sequential metamodeling (bottom left) and AEMOO (bottom right).

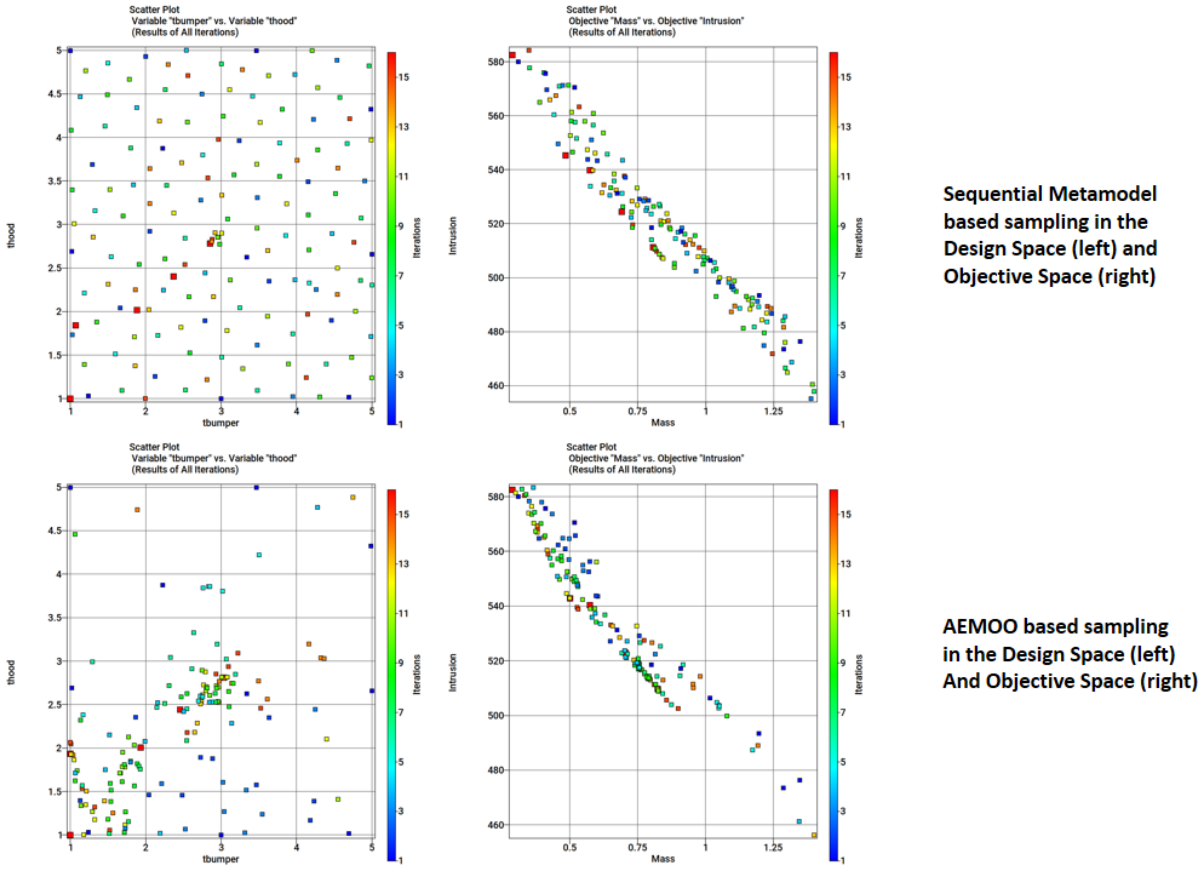

Fig.3: Comparison of sample distribution in the design space (left) and the objective space (right) for sequential metamodel-based optimization and AEMOO.

It is evident from Fig.2: that AEMOO outperforms the current sequential metamodel-based method despite its partial implementation. At iteration 5, a large part of the AEMOO-based Pareto front dominates the sequential metamodel-based front. The same is true for the middle part of the Pareto front at iteration 10 although the sequential metamodel provides a slightly better spread at this point. At the final 15th iteration, AEMOO has slightly better spread and also dominates some parts of the sequential metamodel-based front. Although the later seems to dominate part of the AEMOO-based Pareto Optimal front, the validation results show these points to be infeasible. Thus the AEMOO-based front seems to be more accurate with relatively fewer infeasible points. This can be attributed to the difference in sampling between the two methods. Fig.3: clearly shows that AEMOO avoids sampling large parts of the design space and focuses on the important regions to improve the accuracy there. This can also be seen from the objective space sampling as most of the AEMOO sampling in latter iterations (red) is focused towards the final Pareto Optimal front, which is not the case during sequential metamodel-based optimization. It should be noted that AEMOO does allow some sampling to take place away from the front as well in order to explore the space for existance of disjoint fronts. It is interesting to note that the results are actually better than the direct optimization results with many more (600 vs 50/100/150) samples.

4.3 Reduced Order Modeling

Reduced Order Modeling (ROM) will be added for approximation of histories and multi-point responses/histories. Applications will include history/field approximation based parameter identification, DynaStats etc. In the future, the ROM implementation will be used as a foundation for several other applications and methods that will be presented in due course. An example of DynaStats using ROM approximation (standard deviation of Von Mises stress for plate impacted by a rigid ball with randomized parameters) is shown below.

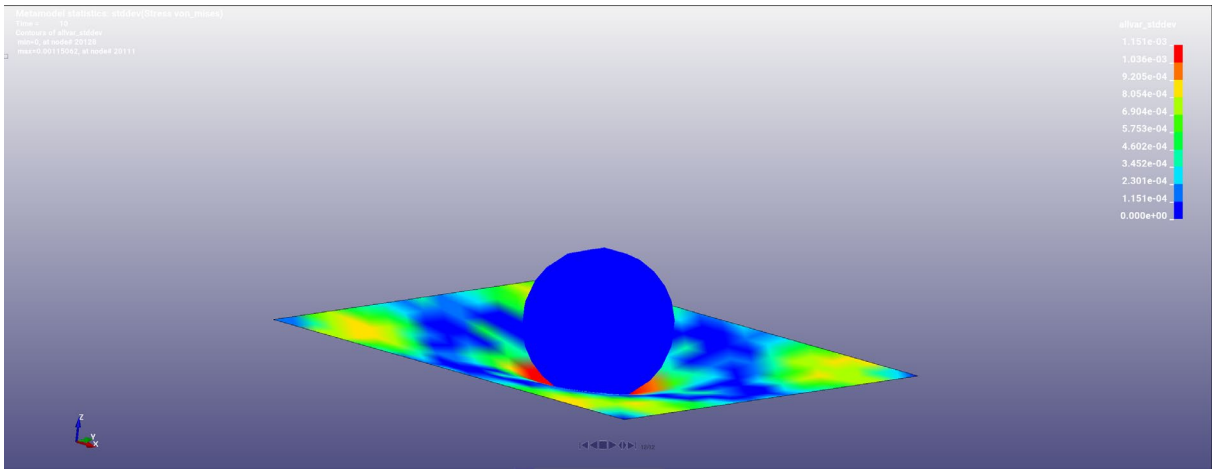

Fig.4: Spatial field approximation of the standard deviation of Von Mises stress using ROM.

4.4 Point Cloud Matching

Methods are currently being implemented for point cloud mapping that have multiple applications, for instance in shape optimization.

4.5 LS-DYNA Results Extraction

The extraction capabilities of LS-OPT will be enhanced in 2022 R2 as well. The integration of LS-Reader in 2022 R1 has provided a foundation to achieve this goal. The plan is to expand the current LS-DYNA interface to support all the result types available in LS-Reader.

5 Closure

The paper again demonstrates the LS-OPT capability of handling reasonably large optimization problems (i.e. 22-variable crash design). More importantly, the results emphasize the need for allowing an individual metamodel type for each response, as well as an automatic selection method for choosing the best metamodel. It therefore demonstrates the benefits of integrating the MOP feature into both the Ansys optimization codes. The extended MOP thus being developed for 2022 R2 should further improve this feature. LS-OPT 7.0 and LS-OPT Pro 2022 R1 enhancements provide a foundation for significant improvements in metamodeling, sample selection and LS-DYNA result extraction. The future 2022 R2 will further build on these to introduce and improve various methods, including the ones discussed in this paper.

6 References

[1] Berndt, D.J., Clifford, J. Using Dynamic Time Warping to Find Patterns in Time Series*, AAAI-94 Workshop on Knowledge Discovery in Databases*, April 26, 1994.

[2] Mueen, A., Keogh Eamonn. Extracting Optimal Performance from Dynamic Time Warping. *KDD 2016*: 2129-2130.

[3] Müller, M, Information retrieval for music and motion. 1. Edition, Springer 2007.

[4] Jekel, C.F., Venter, G., Venter, M.P., Stander, N. and Haftka, R.T. Similarity measures for identifying material parameters from hysteresis loops using inverse analysis. *International Journal of Material Forming.* https://doi.org/10.1007/s12289-018-1421-8, July 14, 2018.

[5] Witowski, K. and Stander, N. Modified Dynamic Time Warping for Utilizing Partial Curve Data to Calibrate Material Models using LS-OPT, 16th LS-DYNA Users Conference, May, 2020.

[6] Most, Thomas and Will, Johannes. (2008). Metamodel of Optimal Prognosis - An automatic approach for variable reduction and optimal meta-model selection. 10.13140/2.1.2194.4007.

[7] Gehre, C. et al; “Objective rating of signals using test and simulation responses”; 21st International Technical Conference on the Enhanced Safety of Vehicles Conference (ESV); Stuttgart; Germany; 2009; Paper 09-0407.

[8] Christian Gehre, PDB – Partnership for Dummy Technology and Biomechanics, Germany. Sebastian Stahlschmidt, DYNAmore GmbH, Germany. Assessment of dummy models by using objective rating methods. Paper Number 11-0216.

[9] Basudhar A, inventor; Livermore Software Technology Corp, assignee. Multi-objective design optimization using adaptive classification. United States patent US 9,852,235. 2017 Dec 26.
[10] Basudhar A. Multi-objective optimization using adaptive explicit non-dominated region sampling. In *11th World Congress on Structural and Multidisciplinary Optimization*, 2015, Sydney, Australia.